Deformable mirror characterization using novel Phase Tilted Interferometry method

Soloviev, Oleg

DOI
10.1117/12.3041952

Publication date
2025

Document Version
Final published version

Published in
Quantitative Phase Imaging XI

Deformable mirror characterization using novel Phase Tilted Interferometry method

Oleg Soloviev[a,b]

[a]Flexible Optical BV, Polakweg 10–11, 2288 GG Rijswijk, the Netherlands
[b]DCSC, ME, TU Delft, Mekelweg 2, 2624 CD Delft, the Netherlands

ABSTRACT

High-accuracy calibration of a deformable mirror is important for the wide range of applications where adaptive optics is used in the feedforward mode or for introducing a precise phase diversity term. While phase shifting interferometry (PSI) can be used for such calibration, it requires expensive equipment and/or cannot be performed on-tool due to space limitations. In this presentation, we demonstrate our novel phase retrieval method from several interferograms with introduced arbitrary tilts (phase tilting interferometry) applied to the calibration of a membrane deformable mirror. As the tilts can be introduced manually by simply misaligning the reference mirror, our method represents an inexpensive and easy-to-use alternative to PSI.

The method first exploits global information to establish the phase tilt parameters using the Zoom FFT to determine the maxima location in the Fourier spectra of the interferogram differences squared. Then, it retrieves the phase locally using the least-squares approach. To decrease the noise print-through in the estimated mirror response functions, linear regression is used on the phases retrieved for several values of the actuator voltages.

Keywords: Adaptive Optics, Interferometry, Phase-Tilting Interferometry, deformable mirror calibration

1. INTRODUCTION

High-accuracy calibration of a deformable mirror is important for the wide range of applications where adaptive optics is used in the feed-forward mode or for introducing a precise phase diversity term. In the frame of 14AMI project,[1] a membrane deformable mirror will be used in a wavefront sensor-less setup inside a semiconductor industry quality check tool in order to correct a residual aberration and to increase the imaging contrast. To meet the tight requirements of the metrology partners, OKO has developed and fabricated a novel deformable mirror with the optimized actuator geometry.[2] Before its use in the actual setup, the mirror should be characterized and calibrated in terms of its response functions and Zernike polynomial, respectively. During its use, the mirror might also require an *in situ* recalibration.

Due to the simplicity of the interferometric measurements, they are also often used "occasionally" (as opposed to the systematic use in the industry) in optical labs, whether for a quick qualitative check or alignment or for an accurate measurement of the aberrations or for *in situ* calibration of adaptive optics.[3] Usually, these occasional-use scenarios do not allow the use of specialized equipment due to the space or budget limitations. This also imposes the limitations on the methods that can be used.

In industry, the Phase-Shifting Interferometry (PSI) -based methods are often used. PSI proceeds by recording several interferograms, introducing exactly known phase shifts that are constant over the whole interferogram area.[4] The shifts are introduced by piezo-actuators, for instance, which should be accurately calibrated to avoid erroneous phase restoration. Accurate actuators are the main limitation of this method, and the calibrated actuators' price makes it expensive. A number of methods are described in the literature able to deal with the imprecision of the phase shift, first for the constant errors,[5–7] later for the vibration-caused (small) tilts[8] and parabolic term,[9] see Refs. 4, 10, 11 for overview.

An often-used alternative method is the single-interferogram method of Takeda[12] and its derivatives. The method uses an intentionally introduced "spatial carrier" (an arbitrary but large enough tilt in the reference beam

Further author information:
E-mail: oleg@okotech.com

Quantitative Phase Imaging XI, edited by Yang Liu, YongKeun Park,
Proc. of SPIE Vol. 13329, 133290J · © 2025 SPIE
1605-7422 · doi: 10.1117/12.3041952

phase) and filtering in the imaging plane to extract the unknown phase. Although it was invented more than 40 years ago, the method is still actively used by researchers due to its simplicity "as is"[3] or with modifications, using classical or neural-network algorithms.[13–16] The main disadvantages of the method and its derivatives are that 1) it limits the maximum curvature that can be sensed with it (the tilted interferogram should not have closed fringes) and 2) it performs low-pass filtering, which introduces an additional source of errors for the interferograms with sharp boundaries and requires additional effort.[17]

In 2005, a method related both to PSI and Takeda's methods was proposed,[18] which was able to extract the phase from three or more interferograms with introduced unknown tilts. The method didn't require any *a priori* knowledge on the tilts except for their sign, and they can be introduced manually by misaligning the reference mirror. The method restored the tilts by analysing the zero-crossing lines of the interferogram differences and proposed a general formula for extracting the phase point-wise from three interferograms with arbitrary phase shifts. The method didn't require the tilts to be large enough, so no closed fringes were present. When used with three interferograms, the extracted phase contained artefacts in a grid shape related to the tilts used, and it was proposed that the method be repeated for other interferogram triples and the results be averaged. This, together with slow and imprecise tilt detection based on the Hough transform, formed the method's main disadvantage.

This presentation demonstrates our novel phase retrieval method from several interferograms with introduced arbitrary tilts (phase tilting interferometry, PTI) applied to calibrating a membrane deformable mirror. As the tilts can be introduced manually by simply misaligning the reference mirror, our method represents an inexpensive and easy-to-use alternative to PSI.

2. METHOD OUTLINE

We consider the following model for the measured multiple interferograms I_n with the introduced linear phase tilts $\delta_n(x)$:

$$I_n(x) = a(x) + b(x)\cos(\phi(x) + \delta_n(x)) + w_n(x), \quad n = 0, \dots, N, \tag{1}$$

$$\delta_n(x) = \tau_n \cdot x + \sigma_n, \tag{2}$$

where $I_n(x)$ is the recorded n-th interferogram (data), $a(x), b(x)$ are the background illumination and the contrast respectively, $\phi(x)$ is the phase being measured, $\delta_n(x)$ are the phase shifts introduced in each measurement, $w_n(x)$ is the measurement noise, x is a (2-dimensional) coordinate, $\cdot$ denotes the scalar product, $\tau_n \in \mathbb{R}^2$ is the tilt vector, and $\sigma_n \in \mathbb{R}$ is the tilt offset. Later, when possible, we shall omit x for brevity.

Unlike in other methods dealing with the phase retrieval from interferograms with random tilts, where the tilts are supposed to be approximately known predefined values, with some variations introduced by, for instance, vibrations, in our approach, the tilts are introduced intentionally and need not be known beforehand, except for the sign of tilt vector with respect to some predefined direction (as explained later). Figure 1 shows a possible optical layout for an optical workshop that allows recording interferograms described by Eqs. (1) and (2). Our method makes use of a known high-quality flatness of the reference mirror, which ensures a good match to the model given by Eq. (2) and does not require the tilts to be known, which allows the introduction of them, for instance, manually.

Our method proceeds sequentially, first using the global constraints of Eq. (2) to estimate the tilts, and then using adapted from PSI phase retrieval algorithms to find the phase ϕ from the local constraints of Eq. (1).

2.1 Tilt detection

To establish the tilts, we note that, disregarding the measurement noise, the interferogram differences $I_n - I_0$ can be represented by a sine of unknown phase multiplied by a sine of a linear term. We can represent a sine as a Hermitian sum of two complex exponents, and thus the Fourier transform of the interferogram difference is some unknown spectrum convolved with a Hermitian sum of two delta-functions, that is a weighted sum with constant coefficients of two shifted copies of the same spectrum. The shift can be found through the autocorrelations.

Mathematically, if

$$\Delta_n = I_n - I_0 = -2b\sin(\delta_n/2)\sin(\phi + \delta_n/2) = \mathrm{i}b \cdot (\mathrm{e}^{\mathrm{i}\delta_n/2} - \mathrm{e}^{-\mathrm{i}\delta_n/2})\sin(\phi + \delta_n/2) \tag{3}$$

then

$$\mathcal{F}(\Delta_n) = \mathrm{e}^{\mathrm{i}\sigma_n/2} G_n(\xi - \tau_n/2) - \mathrm{e}^{-\mathrm{i}\sigma_n/2} G_n(\xi + \tau_n/2), \tag{4}$$

where $G_n(\xi) = \mathcal{F}(\mathrm{i}b\sin(\phi + \delta_n/2))$.

Auto-correlation of this spectrum should have visible maxima. Autocorrelation corresponds to the Fourier of the absolute value squared, so one has

$$\begin{aligned}
\mathcal{F}(\Delta_n^2) &= \mathcal{F}(\Delta_n) \star \mathcal{F}(\Delta_n) \\
&= G_n(\xi - \tau_n/2) \star G_n(\xi - \tau_n/2) + G_n(\xi + \tau_n/2) \star G_n(\xi + \tau_n/2) \\
&\quad - \mathrm{e}^{-\mathrm{i}\sigma_n} G_n(\xi - \tau_n/2) \star G_n(\xi + \tau_n/2) - \mathrm{e}^{\mathrm{i}\sigma_n} G_n(\xi + \tau_n/2) \star G_n(\xi - \tau_n/2) \\
&= 2H_n(\xi) - \mathrm{e}^{-\mathrm{i}\sigma_n} H_n(\xi - \tau_n) - \mathrm{e}^{\mathrm{i}\sigma_n} H_n(\xi + \tau_n) \\
&= 2H_n(\xi) + \mathrm{e}^{-\mathrm{i}(\sigma_n + \pi)} H_n(\xi - \tau_n) + \mathrm{e}^{\mathrm{i}(\sigma_n + \pi)} H_n(\xi + \tau_n),
\end{aligned} \tag{5}$$

wehere $\star$ denotes the correlation operation and $H_n(\xi) \equiv G_n(\xi) \star G_n(\xi)$. This equation is a weighted sum with constant coefficients of three shifted copies of $H_n(\xi)$. For $H_n(\xi)$ is a hermitian function with $H_n(0)$ real and positive, the position of the side maximum of the absolute value of the autocorrelation gives a good approximation to the tilt τ_n, and its argument in that position provides σ_n.

In this work, we have used the Zoomed-FFT algorithm[19,20] to find the maxima values and their position with subpixel accuracy.

Due to the Hermitian nature of the spectra of the interferogram differences squared, the sign of the tilt cannot be determined, and the algorithm needs additional information on the half-plane in the Fourier domain where the maximum of $\mathcal{F}(\Delta_n^2)$ should be located. When the tilt signs are unknown, the phase retrieval algorithm may return the correct phase with a random sign for three input interferograms or the wrong phase for four or more input interferograms.

To ensure the tilt signs are correct, we have used a simple approach of selecting the interferogram with the maximal positive horizontal tilt as the zeroth interferogram I_0 and thus selecting the maxima only from the negative x-half-plane.

2.2 LS PSI phase retrieval

After the tilts are detected, we can consider Eq. (1) at every pixel as a PSI problem. To solve this problem, we used the least-squares PSI approach.

Denote $u = \frac{1}{2}(x + \mathrm{i}y) = \frac{1}{2}b\mathrm{e}^{\mathrm{i}\phi}$ and $d_n = \mathrm{e}^{\mathrm{i}\delta_n}$, $u, \delta_n \in \mathbb{C},\ n = 1, \ldots, N$. Then

$$I_n = \Re(a + 2ud_n) + w_n = u \cdot d_n + \bar{u} \cdot \bar{d_n} + a + w_n,\ n = 1, \ldots, N. \tag{6}$$

If $N \geq 3$, we obtain an (overdetermined for $N > 3$) noisy linear system of equations with complex coefficients

$$A \begin{pmatrix} u \\ \bar{u} \\ a \end{pmatrix} = \begin{pmatrix} I_1 \\ \vdots \\ I_N \end{pmatrix},$$

where A is given by

$$A = \begin{pmatrix} d_1 & \bar{d_1} & 1 \\ \vdots & \vdots & \vdots \\ d_N & \bar{d_N} & 1 \end{pmatrix},$$

and we treat u and $\bar{u}$ as independent variables. Note that matrix A, if multiplied by $\Pi_n d_n$, produces three columns of the Vandermonde matrix, and thus it has rank 3 if there are three different d_n.

If $\hat{u}$ is the LS solution of the system, the phase $\hat{\phi} = \arg \hat{u}$, and the original problem is reduced to solving this linear system of equations, which least squares solution is given by the Moore-Penrose formula

$$\begin{pmatrix} \hat{u} \\ \bar{\hat{u}} \\ a \end{pmatrix} = (A^* A)^{-1} A^* \begin{pmatrix} I_1 \\ \vdots \\ I_N \end{pmatrix},$$

where A^* denotes the conjugate-transposed A.

To simplify the calculations (as we need to get this matrix pseudo-inverse in every point of the interferogram), we, after some calculations, write A^*A as

$$A^* A = \begin{pmatrix} N & \bar{s_2} & \bar{s_1} \\ s_2 & N & s_1 \\ s_1 & \bar{s_1} & N \end{pmatrix},$$

where $s_i = \sum_n d_n^i,\ i = 0, 1, 2$ (we could have written $s_0 = N$), and

$$A^* \begin{pmatrix} I_1 \\ \vdots \\ I_N \end{pmatrix} = \begin{pmatrix} \sum_n \bar{d_n} I_n \\ \sum_n d_n I_n \\ \sum_n I_n \end{pmatrix}.$$

Note that if d_n are N complete circular points (that is $d_n^N = 1\ \forall n$) than we have $A^*A = N\mathbf{I_N}$, where $\mathbf{I_N}$ is the identity matrix of size $N \times N$, and the phase is given by simple formula

$$\hat{\phi} = \arg \sum_n \bar{d_n} I_n,$$

which is known in the literature as N-bin algorithm.[4]

In the general case,

$$(A^* A)^{-1} = \frac{1}{2\Re(s_1^2 \bar{s_2}) - N(2|s_1|^2 + |s_2|^2) + N^3} \cdot \begin{pmatrix} N^2 - |s_1|^2 & \bar{s_1}^2 - N\bar{s_2} & s_1\bar{s_2} - N\bar{s_1} \\ s_1^2 - Ns_2 & N^2 - |s_1|^2 & \bar{s_1}s_2 - Ns_1 \\ \bar{s_1}s_2 - Ns_1 & s_1\bar{s_2} - N\bar{s_1} & N^2 - |s_2|^2 \end{pmatrix}, \tag{7}$$

which can be used to find $\hat{u}$ and $\hat{a}$. Note that although the denominator is a real number, we need to calculate it anyway, as we cannot be sure it's always positive.

3. RESULTS OF THE MIRROR CALIBRATION

3.1 Interferogram registrations

We have used the following set-up (see Fig. 1) to obtain the mirror interferograms. A He-Ne laser with a microscopic objective and pin-hole filtering was used as a point source. The collimated beam was obtained with 700mm 3" lens, and separated into two arms using a wedge beamsplitter. The pellicle beam splitters directed the reflected beams towards the imaging camera and lens L2 with a focal length of 50mm, which forms an image of the DM aperture on the camera. The plane of the aperture was optically conjugated to the camera chip plane.

The tilts τ_l for the PTI method were introduced manually in the reference arm. For each of the tilts, we applied the same sequence of control signals and recorded the interferograms. The control signal sequence represented a linearly increasing voltage $-1 : \Delta V : 1$ applied to a single actuator # n, while holding the rest of the actuators at the "bias" level b:

$$v_m = [b, \ldots, b, -1 + m\Delta V, b, \ldots, b]. \tag{8}$$

In addition, we have recorded the initial shape (corresponding to the control $[-1, \ldots, -1]$) for each of the tilts. This resulted in total $L(1 + \times M \times N)$ interferograms $I_{l,m,n}$ (see Fig. 2). Each of the interferograms was obtained through averaging of K frames to reduce the noise effects and saved in one "HDF5" file for further analysis.

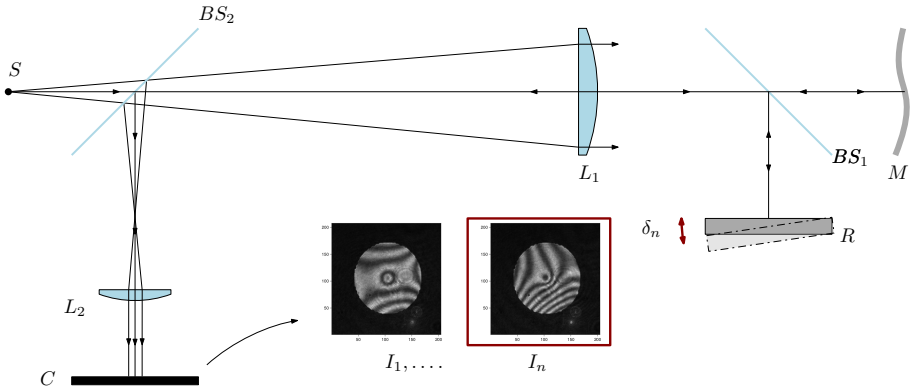

Figure 1: Schematic of the setup used to obtain the phase-tilted interferograms. Point source S was obtained by spatially filtering a focused with a microscopic objective He-Ne laser (not shown). 3" 700 mm lens L_1 formed a collimated beam which was divided by wedge beam-splitter BS_1 into a measurement and reference arms. After reflection from the flat reference mirror R and deformable mirror M, the arms are recombined again by BS_1 and folded by pellicle beam splitter BS_2 towards camera C. 1" 50mm lens L_2 with L_1 form Keplerian telescope which reimages the mirror plane M to the camera chip plane C. Arbitrary tilts δ_n are introduced in the reference beam by manually adjusting the screws of the mirror R mount, and interferogram I_n is recorded.

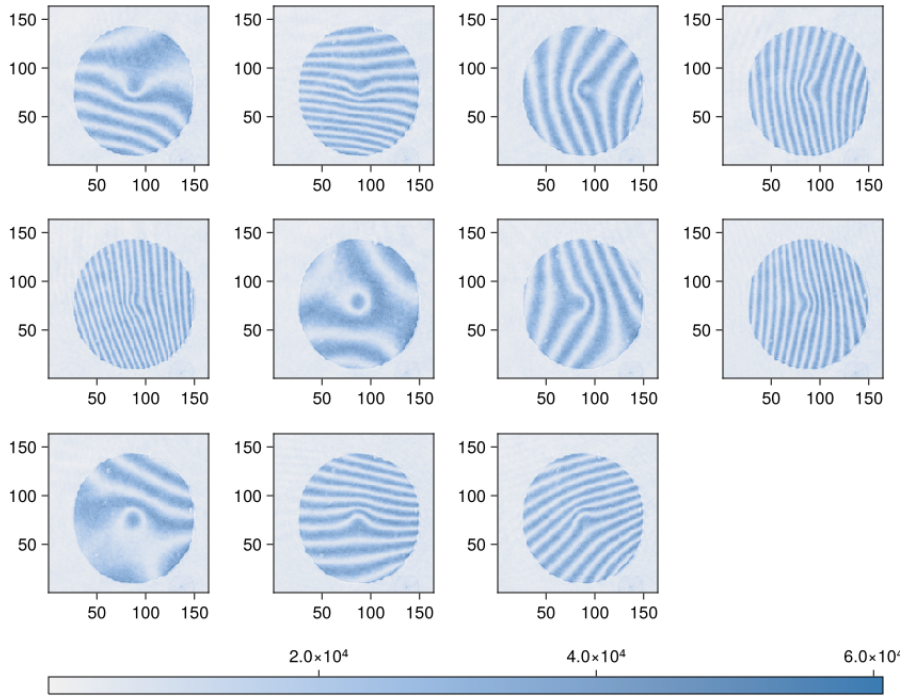

Figure 2: Example of interferograms obtained for the mirror calibration $I_{l,m,n}$ for $m = M, n = 1$. Each individual interferogram is a 16-bit TIFF image.

3.2 Phase extraction

For each pair of (m, n) we have used the algorithm of Section 2 to extract the phase. We have used a manually drawn ellipse on top of one of the interferometric images as the aperture mask for all measurements. As the algorithm needs the tilt signs to be known, we have used the selected tilt with maximal positive horizontal component as the reference interferogram, so all the tilt vectors τ_l were located in the negative half-plane of the spectra of the interferogram differences (see Fig. 3b).

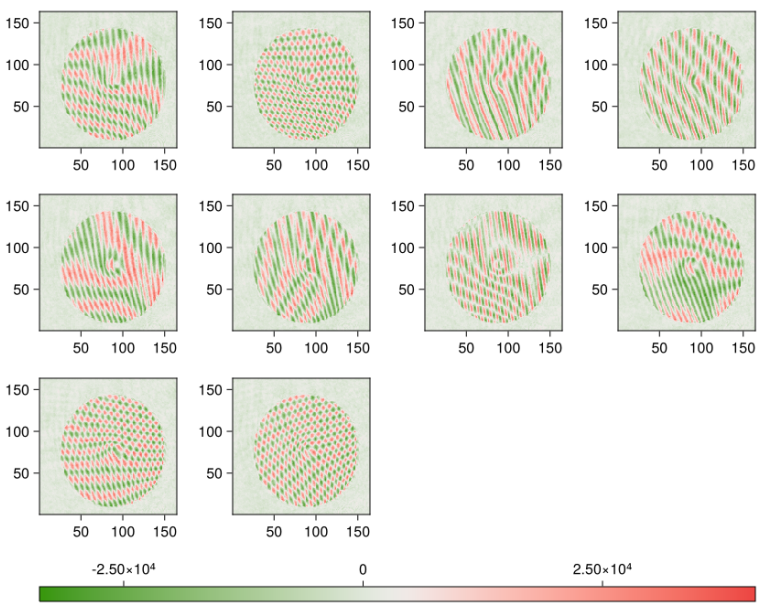

(a) $I_{l,M,1} - I_{0,M,1},\ l = 1, \ldots, L$

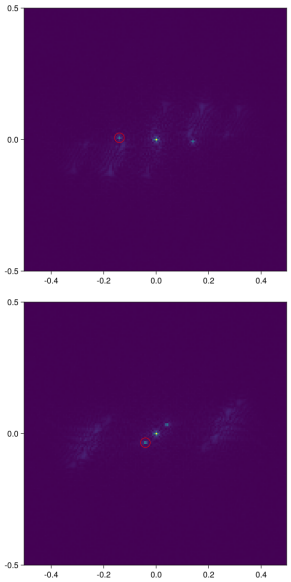

(b) $\mathcal{F}\left((I_{l,M,1} - I_{0,M,1})^2\right)$ for $l = 1, 4$

Figure 3: Interferogram differences and examples of the Fourier spectra of the interferogram differences squared. The maxima selected by the algorithm in the spectra are marked with a red circle.

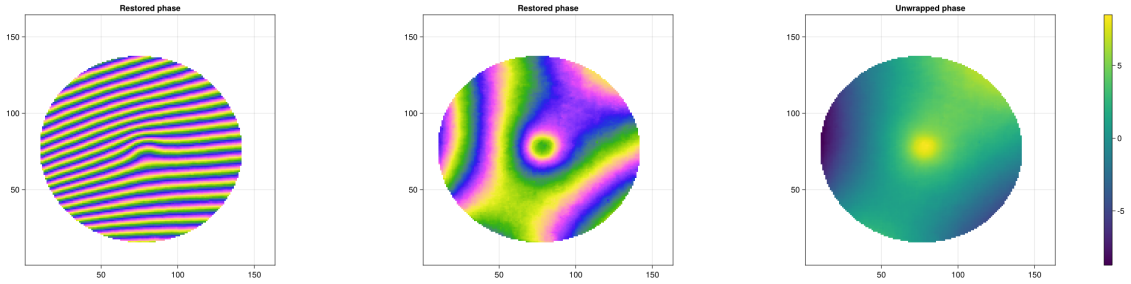

Figure 4: Extracted by the algorithm phase $\phi_{0,M,1}$ (l); phase with the reference tilt removed $\phi_{0,M,1} - \delta_5$ (c); unwrapped phase $\psi_{M,1}$ (r).

In the registered interferograms, the interferogram without any tilt introduced is given by the sixth image (that is $l = 5,\ I_{5,M,1}$ in Fig. 2), but the algorithm returns the phase corresponding to $l = 0$, so we need to remove the reference tilt from the extracted phase; the phase is then unwrapped inside the aperture mask using the LS-unwrapping algorithm and saved as $\psi_{m,n}$ (see Fig. 4).

3.3 Response extraction

To get the mirror response for a given actuator number n, we combine all its extracted phases $\{\psi_{n,m},\ m = 1, \ldots, M\}$ (see Fig. 5). Ideally, they should represent a sequence of linearly scaled copies of the same response function plus the bias shape:

$$\psi_{n,m} \approx v_m r_n(x) + b r_0(x). \tag{9}$$

However, due to the vibrations present in the system, there might be some residual tilt and piston. As the membrane mirror responses are all equal to zero on the aperture edge, we can correct for these residual linear terms by considering the response function increments $\psi_{m+1,1} - \psi_{m,1},\ m = 1, \ldots, M-1$, and finding the best fitting linear function to them (see Fig. 5).

Finally, after removing the residual linear terms from the actuator phases, one can use linear regression to calculate response function $r_n(x)$ and bias $r_0(x)$ from Eq. (9) (see Fig. 6). Finally, the phase responses are

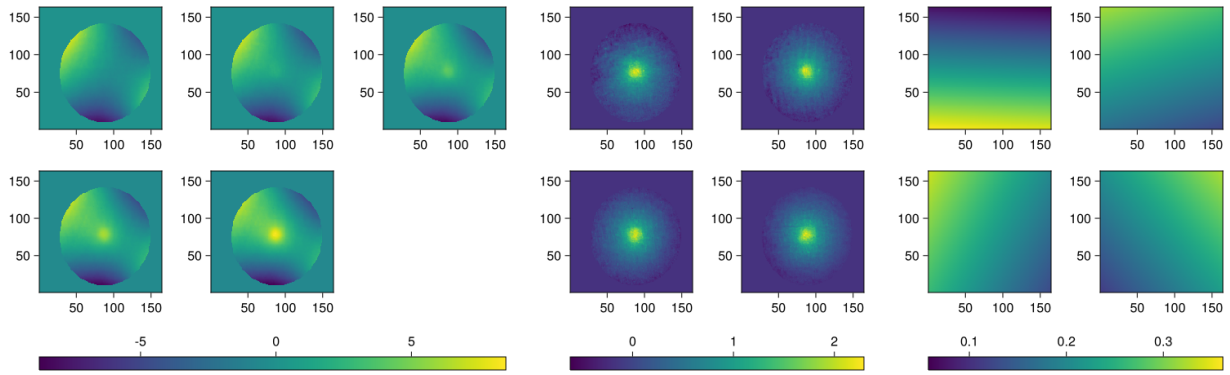

Figure 5: Extracted by the algorithm phases $\psi_{m,1},\ m = 1, \ldots, 5$ (l); their masked increments $\psi_{m+1,1} - \psi_{m,1},\ m = 1, \ldots, 4$ (c); extracted from the increments remaining linear terms (r).

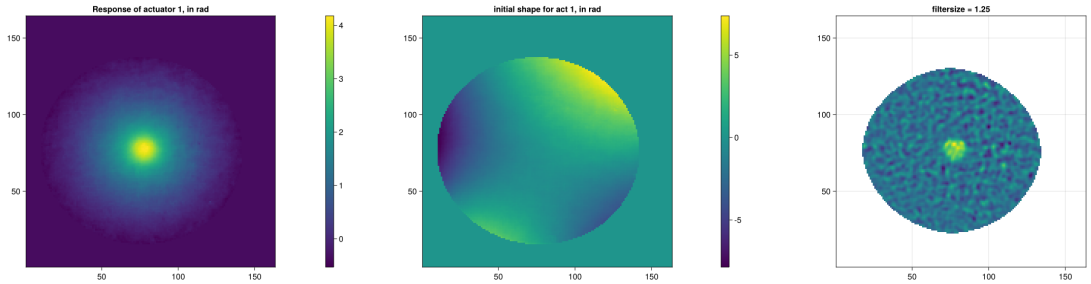

Figure 6: Restored phase response function of the first actuator $r_1(x)$ (l), initial mirror shape $r_0(x)$ (c); Laplacian of filtered with Gaussian filter response Δr_1 (r).

converted to the mirror shape responses by multiplying them by $-\lambda/\pi$ (se Fig. 7).

3.4 Results validation

For a quick results validation, we have calculated the Laplacian of the responses $\Delta r_n(x)$ (to remove the noise influence, the responses were smoothed using a Gaussian filter with a kernel size of 1.25 pixels). According to the

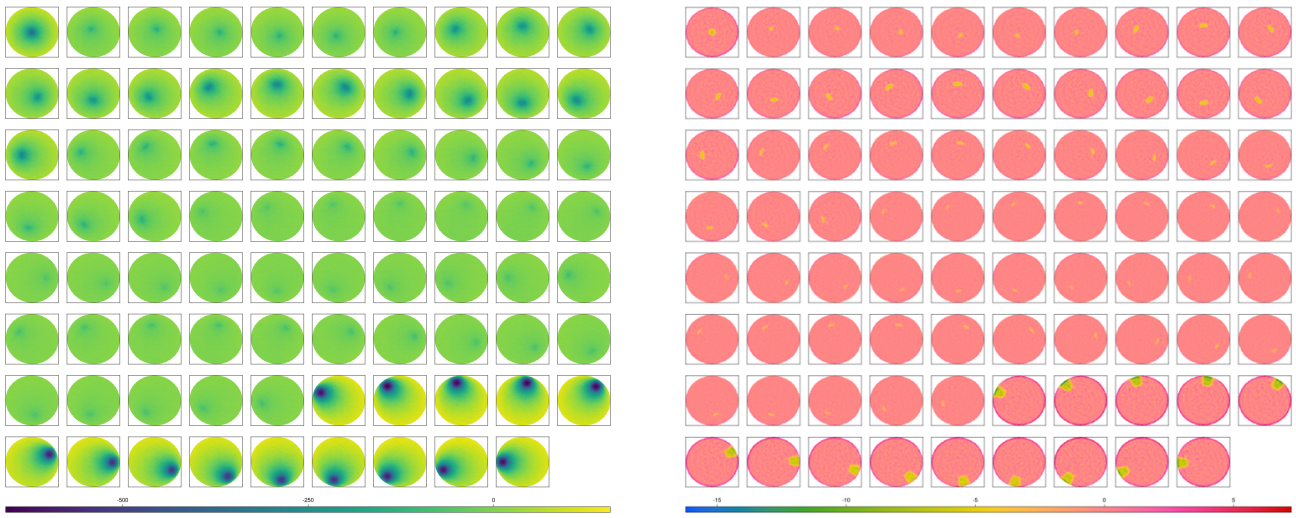

Figure 7: Restored shape responses functions of the mirror, in nm (l) and Laplacian of filtered with Gaussian filter responses(r).

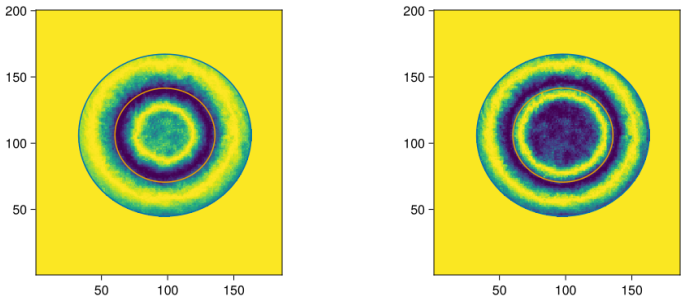

Figure 8: Checking the alignment of the assembled mirror by combined ring responses

theoretical model[21] of the membrane mirror shape $w(x)$, it is governed by the Poisson equation $\Delta w(x) \propto V^2(x)$, where $V(x)$ is the voltage distribution on the mirror actuators, the Laplacian of a response function should return the actuator characteristic function, and this is clearly visible on the retrieved responses (see Figs. 6 and 7). The uniformity of the amplitudes of the response Laplacians confirms the good alignment of the mirror membrane with respect to the actuator structure. In addition, the alignment is also verified by the concentricity of the combined responses of the actuators belonging to a certain ring, see Fig. 8.

Finally, we have calculated the approximation of the first 25 Zernike polynomials with the retrieved responses; see Fig. 9 for some examples. Due to the noisy input interferograms and noise print-through in the retrieved responses, we could not validate the shape of the approximation errors against the theoretical prediction of Reference 2. However, the uniformity of the error shape confirms that the calculated approximation coefficients can be used for feed-forward Zernike generation.

4. CONCLUSIONS

We have presented a method of inexpensive interferometric calibration of a deformable mirror. The method uses several interferograms with purposely introduced arbitrary tilts and is not sensitive to vibrations. The method was demonstrated on example of characterisation of a membrane deformable mirror.

ACKNOWLEDGMENTS

The project is supported by the Chips Joint Undertaking and its members, including the top-up funding by RVO (The Netherlands Enterprise Agency).

REFERENCES

[1] Horizon Europe, "14 Angstroms Module Integration (14AMI)," online, Grant agreement ID: 101111948 (May 2023).
[2] Soloviev, O., "Optimization of deformable mirror actuator geometry using machine learning methods," in [*Adaptive Optics and Wavefront Control for Biological Systems XI*], *Proc. SPIE 13328* (2025).
[3] Antonello, J., Wang, J., He, C., Phillips, M., and Booth, M., *Interferometric calibration of a deformable mirror* (Mar. 2020).
[4] Surrel, Y., [*Fringe Analysis*], 55–102, Springer Berlin Heidelberg, Berlin, Heidelberg (2000).
[5] Greivenkamp, J. E., "Generalized Data Reduction For Heterodyne Interferometry," *Optical Engineering* **23**, 350–352 (aug 1984).
[6] Okada, K., Sato, A., and Tsujiuchi, J., "Simultaneous calculation of phase distribution and scanning phase shift in phase shifting interferometry," *Optics Communications* **84**, 118–124 (jul 1991).
[7] Du, H., He, Z., Ma, P., Chen, X., and Yin, P., "Phase-shift extraction of multiple-frame randomly phase-shifted interferograms by analysis of the amplitude of the analytic signal," *Applied Optics* **59**(31), 9844 (2020).
[8] Chen, M., Guo, H., and Wei, C., "Algorithm immune to tilt phase-shifting error for phase-shifting interferometers," *Applied Optics* **39**, 3894 (aug 2000).

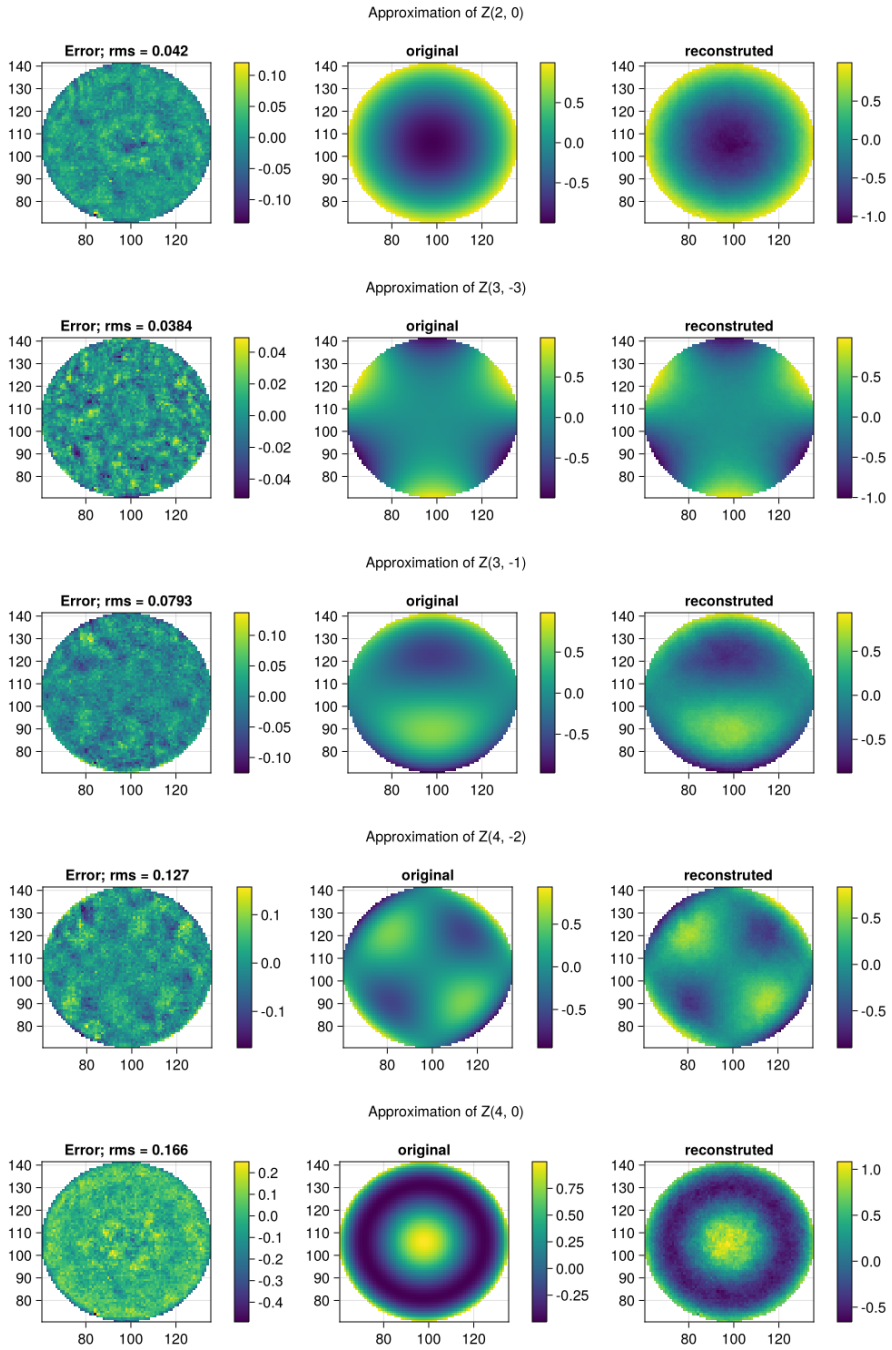

Figure 9: Approximations (right column) of certain Zernike modes (middle column) by the measured response functions of the prototype mirror and the remaining error (left column). The "original" polynomials are normed to 1 a.u. in amplitude.

[9] Kihm, H., "Phase recovery of high numerical-aperture spherical surfaces in tilt phase-shift interferometry," *Optical Engineering* **55**, 074101 (jul 2016).

[10] Servin, M., Estrada, J. C., and Quiroga, J. A., "The general theory of phase shifting algorithms," *Optics Express* **17**, 21867 (nov 2009).

[11] Servin, M., Padilla, M., Paez, G., and Garnica, G., "Universal phase-shifting algorithm (UPSA) for nonuniform phase-step demodulation and null-testing criterion for phase accuracy gauging," *Optics and Lasers in Engineering* **158**, 107180 (nov 2022).

[12] Takeda, M., Ina, H., and Kobayashi, S., "Fourier-transform method of fringe-pattern analysis for computer-based topography and interferometry," *J. Opt. Soc. Am.* **72**, 156–160 (Jan 1982).

[13] Singh, M. P., Singh, M., and Khare, K., "Single shot interferogram analysis for optical metrology," *Applied Optics* **53**(29), 6713 (2014).

[14] Dong, Z. and Chen, Z., "Advanced Fourier transform analysis method for phase retrieval from a single-shot spatial carrier fringe pattern," *Optics and Lasers in Engineering* **107**(February), 149–160 (2018).

[15] Khorin, P. A., Dzyuba, A. P., Chernykh, A. V., Georgieva, A. O., Petrov, N. V., and Khonina, S. N., "Neural Network-Assisted Interferogram Analysis Using Cylindrical and Flat Reference Beams," *Applied Sciences* **13**, 4831 (apr 2023).

[16] Zhang, T., Shi, R., Shao, Y., Chen, Q., and Bai, J., "Single-frame noisy interferogram phase retrieval using an end-to-end deep learning network with physical information constraints," *Optics and Lasers in Engineering* **181**(July), 108419 (2024).

[17] Roddier, C. and Roddier, F., "Interferogram analysis using Fourier transform techniques," *Applied Optics* **26**, 1668 (may 1987).

[18] Soloviev, O. and Vdovin, G., "Phase extraction from three and more interferograms registered with different unknown wavefront tilts," *Optics Express* **13**(10), 3743 (2005).

[19] Bluestein, L., "A linear filtering approach to the computation of discrete Fourier transform," *IEEE Transactions on Audio and Electroacoustics* **18**, 451–455 (dec 1970).

[20] Jurling, A. S., Bergkoetter, M. D., and Fienup, J. R., "Techniques for arbitrary sampling in two-dimensional Fourier transforms," *Journal of the Optical Society of America A* **35**, 1784 (nov 2018).

[21] Vdovin, G. V., Middelhoek, S., and Sarro, P. M., "Technology and applications of micromachined silicon adaptive mirrors," *Optical Engineering* **36**, 1382 – 1390 (May 1997).